HHS Public Access

Author manuscript

J Phys Chem B. Author manuscript; available in PMC 2016 November 30.

Published in final edited form as:

J Phys Chem B. 2016 September 15; 120(36): 9654–9660. doi:10.1021/acs.jpcb.6b06775.

Lowered pH Leads to Fusion Peptide Release and a Highly-dynamic Intermediate of Influenza Hemagglutinin

Xingcheng Lin[†,‡,¶], **Jeffrey K. Noel**[§,‖,¶], **Qinghua Wang**[⊥], **Jianpeng Ma**[†,⊥,#], and **José N. Onuchic**[†,‡,@,*]

[†]Center for Theoretical Biological Physics, Rice University, Houston, TX

[‡]Department of Physics and Astronomy, Rice University, Houston, TX

[§]Max Delbrück Center for Molecular Medicine, Berlin, Germany

[‖]Fritz Haber Institute of the Max Planck Society, Berlin, Germany

[⊥]Verna and Marrs McLean Department of Biochemistry and Molecular Biology, Baylor College of Medicine, Houston, TX

[#]Department of Bioengineering, Rice University, Houston, TX

[@]Departments of Chemistry and Biosciences, Rice University, Houston, TX

Abstract

Hemagglutinin (HA), the membrane-bound fusion protein of the Influenza virus, enables the entry of virus into host cells via a structural rearrangement. There is strong evidence that the primary trigger for this rearrangement is the low pH environment of a late endosome. To understand the structural basis and the dynamic consequences of the pH trigger, explicit-solvent molecular dynamics simulations were employed to investigate the initial stages of the HA transition. Our results indicate that lowered pH destabilizes HA and speeds up the dissociation of the fusion peptides (FPs). A buried salt-bridge between the N-terminus and ASP_{112} of HA stem domain locks the FPs and may act as one of the pH sensors. In line with recent observations from simplified protein models, we find that, after the dissociation of FPs, a structural order-disorder transition in a loop connecting the central coiled-coil to the C-terminal domains produces a highly mobile HA. This motion suggests the existence of a long-lived asymmetric, or "symmetry-broken" intermediate during the HA conformational change. This intermediate conformation is consistent with models of hemifusion, and its early formation during the conformational change has implications for the aggregation seen in HA activity.

Graphical abstract

Phone: (713)348-4197, jonuchic@rice.edu.

[¶]These authors contributed equally to this work

Supporting Information Available

This material is available free of charge via the Internet at http://pubs.acs.org/.

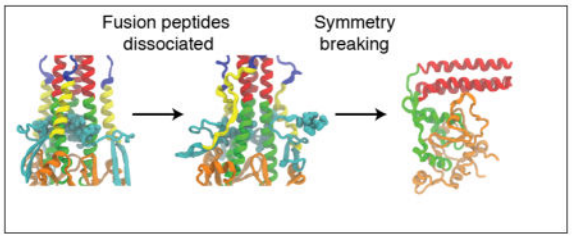

Introduction

Hemagglutinin (HA) is a viral membrane protein responsible for entry of influenza viruses into human cells.[1] Recognition of the receptor-binding domain by the sialic acid receptors on the outer membrane of a host cell triggers endocytosis of the virus. Then, reduction of pH inside the endosome triggers a large conformational rearrangement of the C-terminal domain HA_2 that results in the fusion of the viral and endosomal membranes and delivery of the viral genome inside the cell. Similar fusion mechanisms are shared by other viral fusion proteins.[2,3] HA_2 has recently been the subject of intense scrutiny because its evolutionary conservation suggests that it can serve as a target for drugs or vaccines effective against a large number of influenza subtypes.[4–6]

The endpoints of the functional HA_2 rearrangement are known from X-ray crystallography. HA is a homotrimer composed of two domains: a globular, receptor-binding domain formed exclusively by HA_1, and an inner stem domain formed primarily by HA_2 with the N- and C-terminal fragments of HA_1 (Fig. 1A). Each monomer contains one chain of HA_1 disulfide bonded to one chain of HA_2. A pre-fusion structure containing both HA_1 and HA_2 shows how HA_1 envelops HA_2 and sterically restricts HA_2 rearrangement.[7] The post-fusion structure of HA_2 was obtained under low pH conditions and trimmed to remove the fusion peptides (FPs).[8,9] Comparison with the pre-fusion structure reveals dramatic changes in secondary, tertiary, and quaternary structure,[8,10] which opens the possibility of long-lived intermediate ensembles. Therefore, any search for structure-based therapeutics is incomplete without an understanding of the paths HA_2 follows during its conformational rearrangement. In this paper, we employ explicit-solvent molecular dynamics simulations to bridge previous studies into a clearer picture of the early events in the HA_2 rearrangement.

To facilitate discussion of the HA_2 rearrangement, the trimer is partitioned into 7 sections identified from crystal structures as regions with distinct structural changes during the transition:[8,10] the fusion peptides (FPs), two beta-strands (TBS) and S1 to S5 (see Fig. 1, and details can be found in ref.[10] and SI). The FP (residues 1 to 20 in each monomer. We note that a recent study suggests the functional FP contains residues 1 to 23.[11]) initially have their N-termini buried in a cavity surrounded by S4. The burial location is termed Loop3-4, because this subset of S4 becomes a loop connecting S3 and S4 in the post-fusion structure. S1 (often called the A-helix) and S2 (often called the B-loop) undergo secondary and tertiary changes, so that instead of connecting back to Loop3-4, they extend the three helix bundle of S3 into S1/S2/S3, moving the N-termini as far as possible from Loop3-4. TBS, S1, and S2 together (residue ID 21 to 75) are abbreviated as the “arms.”

Previously, both experimental and computational studies have highlighted the role of the late endosome's lowered pH in initiating the conformational change. Mechanistically, a pH drop can create electrostatic repulsion between the three monomers of HA_1 and encourage their dissociation, relieving their steric inhibition of the HA_2 rearrangement.[12,13] Importantly, there are titratable residues proximal to the burial pocket of the FPs in HA_2 that may encourage their removal.[14] Beyond the pH trigger, the paths that HA follows during the conformational rearrangement were recently studied for the first time[10] with dual-basin structure-based simulations (SBS).[15,16] These simplified protein folding models were parameterized using the pre- and post-fusion crystal structures of HA_2. These simulations yielded a novel view of the HA_2 rearrangement by indicating a highly dynamic intermediate ensemble after fusion-peptide release. This long-lived intermediate ensemble was characterized by a symmetry-breaking of the trimeric structure, which we called a "symmetry-broken intermediate" (SBI).[10]

Since the simulations presented here are motivated in part by the results of previous simplified models, it is important to review the relevant findings from these previous SBS. The SBS[10] have indicated that an order-disorder transition of Loop3-4 (Fig. 1A,B) is integral to initiating the HA_2 rearrangement. The disorder in Loop3-4 disrupts the sites where the S1 monomers and FPs are docked onto S4 and encourages their dissociation.[10] After FP dissocation, the S4 homo-trimer undergoes a symmetry-breaking as one monomer of S4 bends anti-parallel to S3 to form its post-fusion contacts, leading to the long-lived SBI configuration. There are two causes of the instability of Loop3-4 in the SBS: 1) the absence of FP creates a void of stabilizing contacts at the interior of HA_2 centered on Loop3-4, and 2) the influence of the final structure in the Hamiltonian causes the Loop3-4 region of S4 to be unstable. Cause 1 in particular requires further scrutiny because the SBS were unable to explicitly include FPs. Cause 2 also deserves a closer look because the structural propensity of Loop3-4 towards a disordered loop may not exist when Loop3-4 is in the context of the pre-fusion structure. In the following we explore the dynamics of the FP and Loop3-4 in the context of the pre-fusion HA_2 with detailed simulations based on transferable explicit-solvent potentials.

Methods

Protonation of titratable residues

The acidic environment in the endosome leads to the protonation of acidic residues of HA. At pH 5 HA_1 becomes strongly positive, likely leading to its dissociation.[14] Because of this, in our simulations we do not explicitly represent most of HA_1. HA_2 also has several acidic residues which need to be assigned protonation states. In this paper we employ constant protonation state MD, as opposed to generalized ensemble constant pH methods.[17] The PROPKA algorithm[18] is used to determine the pKa of a residue in the context of a static structure. PROPKA takes into account a residue's protein and solvent environment to determine pKa. To determine the protonation state of a residue for production simulations, we computed the pKa of a residue over an ensemble of structures generated from a 1 μs equilibration simulation starting at the crystal structure using a putative pH 4.5 protonation state taken from ref.[14] The residues with a pKa above 4.5 in over half of the snapshots were

protonated and the protonation state held constant during a kinetic simulation. ASP_{112} was predicted to be unprotonated in the presence of FP and protonated after the dissociation of FP. In fact, at pH 4.5, ASP_{112} is the only residue that is predicted to change upon dissociation of the FP. Protonation state prediction for the later stage simulations were trained on the previous about 1 μs of simulation. That is, simulation set 2 (HA_2 residues 21–175 at pH 5.0) was trained on 1 μs of the full system at pH 4.5, and simulation set 3 (HA_2 residues 76–175 at pH 5.0) was trained on the last 1 μs of simulation set 2. Protonation states for titratable residues for all three sets of simulations are listed in Supporting Table 2.

As just described, in our simulations the protonation state of the titratable residues does not change during the time of a simulation. More sophisticated methods exist which allow protonation/deprotonation events during the simulation in order to approach a thermodynamically-correct ensemble.[17] From a kinetic point of view, these individual protonation events should take longer than the μs-scale simulation length. A rate of protonation can be estimated using a diffusion-limited Smoluchowski encounter model[19,20] with the Grotthuss diffusion rate, and the assumptions that every residue is a perfect receptor and fully solvated. In this fastest ideal case, the rate of proton transfer at pH 5 would take 1–5 μs (see Supporting Information). Thus, the approximation that the protonation states do not change in our simulation is valid, and any errors lie in the quality of the protonation state predictions.

Simulation details

Three sets of explicit-solvent simulations were performed at physiological temperature (310K) using the Anton supercomputer.[21] The protein was solvated with the TIP3P water model, Na^+ and Cl^- ions were used to neutralize and mimic the endosomal ionic environment of HA molecule, with a physiological concentration of 0.15 M. The simulations were performed with a time step of 2.0 fs. The forcefield CHARMM22*[22] was used. CHARMM22* was created to correct the overstabilization of helices in CHARMM22/CMAP and to more accurately describe salt-bridge interactions.[22] HA was oriented to fit into a rectangular simulation box. To prevent the protein molecule from tumbling and touching its periodic image, restraints were added to the most distant backbone residues (residue ID 76, 77, 174, 175; each monomer). The molecule was initially aligned with the Z-axis. A harmonic restraint was then applied in the X-Y plane of C-terminal residues (residue ID 174, 175; each monomer) with force constant 0.2 kcal/mol/$Å^2$. A weaker constraint was applied to the N-terminal residues (residue ID 74, 75; each monomer) in the X-Y plane with force contant 0.00025 kcal/mol/$Å^2$. The difference in strength was to reduce the energetic penalty for HA_2 to rotate about its central axis. In addition, a weak harmonic restraint was added to the Z-axis of C-terminal residues (residue ID 174, 175; each monomer) with force constant 0.0016 kcal/mol/$Å^2$ to mimic the fact HA_2 was bound to the viral membrane. Except for the N-termini of HA_2, the termini were capped with ACE (acetyl group) and NME (methylamine) because they were cut from the full protein (C-termini of HA_2 cut from its transmembrane domain; peptide of HA_1 from the complete HA_1). The Multigrator integrator[23] was used in conjunction with the Nose- Hoover thermostat[24,25] and the MTK barostat[26] at 1 bar with time interval of 240 ps. The long-range electrostatics was treated with the Gaussian split Ewald method.[27]

The dissociation of FPs was too slow at 310 K to generate statistics when the FP pocket was stabilized by salt bridges. Thus, a higher temperature of 398K was used to speed up the barrier crossing.[28] Even if no FP dissociated, a simulation was stopped after a maximum of 200 ns. These simulations were performed using Gromacs 5.0.4.[29] PME (Particle Mesh Ewald) was used for long-range electrostatics[30] with a Fourier grid spacing of 0.12 nm. Temperature was maintained using the velocity rescaling algorithm.[31] Pressure was coupled at 1.0 bar with Parrinello-Rahman algorithm[32,33] with time constant 2.0 ps. A symmetric dodecahedron box was used and, thus, no harmonic restraint was needed to maintain the orientation of the protein molecule.

Results

Protonation of titratable residues speeds the dissociation of FPs

The FPs are initially buried in a pocket surrounded by hydrophobic residues of HA_2 (Fig. 1) and must be released in order to interact with membranes. Our simulations start from the crystal structure of HA including the complete stem domain HA_2 and the three beta strands (residue ID 10–18 of three monomers) of HA_1 that form disulfide bonds with HA_2 (Fig. 1(B)). 26 residues in each monomer were protonated according to our training scheme at pH 4.5 (see Methods and Supporting Information for details). 12 of these residues are within 8 Å of a FP (one Debye-Hückel screening length at a salt concentration of 150 mM). Notably, a strong electrostatic interaction is formed between ASP_{112} and the N-terminus of the FP in the crystal structure. PROPKA predicts that in the presence of a FP ASP_{112} stays charged, while after FP dissociated it becomes neutral. Thus, protonation of ASP_{112} can act as a switch that breaks the meta-stable salt-bridge-like interaction and reduce the stability of FPs. Evidence for the stabilizing effect of negatively charged ASP_{112} comes from experiments showing that the mutation of ASP_{112} raises the fusion pH and speeds up the fusion reaction.[35–37] These experiments also highlighted the kinetic importance of the FP region by showing that mutations in FP-HA_2 interactions that raised the fusion pH could not be rescued by stabilizing mutations elsewhere.

In order to investigate the kinetics of FP dissociation, we performed constant temperature (310K) MD simulations starting from the pre-fusion crystal configuration with varying protonation states. These simulations indicate that protonation of ASP_{112} along with the PROPKA predictions leads to FP release on the sub-μs time scale (Fig. 1C). The trajectory highlighted in Fig. 1C shows a first FP leaving the HA_2 hydrophobic pocket completely at 850 ns, and a second FP partially leaving near the end of the 2 μs simulation. In total, 3 out of 4 simulations show at least one FP dissociated, where the first FP left at an average of 500 ns (Supporting Information).

To identify the barrier of FP release with the protonation of ASP_{112}, we performed simulations with charged ASP_{112} where the salt bridge between the N-terminus of the FPs and ASP_{112} is initially intact. In this situation a FP is more stable, so a temperature higher than physiological temperature (T = 398K) is used to increase the kinetics of FP dissociation (Fig. 1D). In 10 simulations with neutral ASP_{112} and HA_2 protonated for pH 4.5, FP release occurs at an average of 25 ns. If only one ASP_{112} is neutralized, the proximate FP is released at an average of 58 ns (not shown in Fig. 1D). However, in 7 simulations with charged

ASP_{112} and HA_2 protonated for pH 4.5, FP release occurs at an average of ≥160 ns. The difference in FP lifetime for the two charge states comes from their disparate routes for FP release. With neutral ASP_{112}, the FP has low affinity for its burial location and can rapidly dissociate while HA_2 is still intact. With charged ASP_{112}, FP burial is more stable than domain S5, and the FPs are only seen to dissociate after S5 has fallen apart. S5 melting opens and destabilizes the FP burial pocket, allowing FP release. A set of 6 control simulations with HA_2 protonated for pH 7 and with neutral ASP_{112} showed a stable S5 and no FP dissociation within 200 ns. Though our ability to discern the dependence of FP stability on ASP_{112} protonation state is hampered by the lower relative stability of the S5 domain, our result suggests that negatively charged ASP_{112} provides significant stability to the FPs. Also, S5 stability is affected by pH. Therefore, the kinetic simulations demonstrate a possible second route for FP dissociation; release after the melting of S5. However, such a route would likely lead to non-fusogenic HA_2 because S5 melting before FP insertion into a host membrane would trap the FPs at the viral surface.[10,38]

Helical structure of Loop3-4 is unstable

While we have shown that protonation of titratable residues can drive the dissociation of the FPs, it is also important to consider how this process is related to the dynamics of Loop3-4, which creates the burial site for the FPs. Loop3-4 undergoes a helix-to-loop conversion between the pre- and post-fusion crystal structures[8,10] and, therefore, is a natural candidate for a conformational switch. In order to investigate the role of Loop3-4 disorder on the HA_2 transition and its interplay with FP dissociation, we monitored the helical order of Loop3-4 during three distinct stages of the HA_2 transition at physiological temperature: Before any FP is released, after all FPs have dissociated, and after the breaking of the S1–S4 interface (Fig. 2). The helical order of a residue is defined as the fraction of time the STRIDE algorithm[39] identifies its secondary structure as helical. Before dissociation of FPs, in the stretch of S3 to S4, only Loop3-4 lacks perfect helical order. This supports the idea that Loop3-4 is structurally unstable compared with the other residues in S3 to S4, consistent with the results from SBS and a secondary structure prediction algorithm.[40] FP dissociation was modeled by taking the ending configuration of the simulation shown in Fig. 1C, deleting the FPs (residue ID 1 to 20), and extending the simulation for 2 μs. Interestingly, after FP dissociation, Loop3-4 becomes almost perfectly ordered. The Loop3-4 ordering may discourage backtracking of the FPs into the burial pocket and enhance the irreversibility of the HA_2 transition. We note that this and subsequent simulations are performed at pH 5.0, which affects the charge state of residues in S1, S2 and S5, but not S3 or S4. The last step, breaking of the S1–S4 interface, leads to complete disordering of Loop3-4.

Breaking of the S1–S4 interface leads to symmetry-breaking

A clear function of HA is to expose the FPs to the host membrane. While S3 and S4 maintain the prefusion interface with the “arms”, S1 and S2 (A-helix and B-loop), the FPs cannot extend away from the viral membrane. Thus, we anticipate that breaking this interface is an important event in the HA molecular rearrangement. Breaking of the S1–S4 interface was not spontaneous within our available timescale (2 μs), so we studied the effects of arm dissociation by deleting the arms from HA_2 and extending the simulation for 6 μs. Note that the FPs are also removed, and thus, these simulations explore the Loop3-4

dynamics in a scenario where the FPs have dissociated before or concommitantly with the arms.

Without the stabilizing contacts of the arms, the Loop3-4 region disorders on the sub-microsecond timescale and initiates a symmetry-breaking of the HA_2 molecule. Whereas in the pre-fusion structure S3 is perpendicular to the viral membrane, after the disordering of Loop3-4, the angle of S3 with respect to the viral membrane (θ_{S3}) can vary significantly on the microsecond timescale (Fig. 3). θ_{S3} undergoes large fluctuations, up to a maximum of 110°. The mean square deviation along θ_{S3} is linear on the submicrosecond time scale giving an effective diffusion coefficient of 7×10^2 deg^2/μs (Fig. 3D).

Sufficiently large motion along θ_{S3} would allow S3 to interact with S5. Such an interface, assuming a rigid S3 and S5, can only be created near $\theta_{S3} \sim 120°$. Since the 5 μs simulation only visited $\theta_{S3} \leq 110°$, we applied a bias towards large θ_{S3}, which led to the configuration shown in Fig. 3B with $\theta_{S3} = 129°$. This configuration resembles the symmetry-broken intermediate (SBI) seen in SBS, which is stabilized by one S3 monomer creating its post-fusion contacts with S5. Unbiased simulations started from this configuration (Fig. 3B left) were stable, i.e. θ_{S3} unchanged and S3/S5 interface maintained, for the length of the simulation (600 ns). A simulation started from the SBI structure predicted in SBS (Fig. 3B right) had the same result. While this analysis cannot discern which SBI is the most likely long-lived state, it does show that an S3/S5 interaction slows the dynamics along θ_{S3} significantly below that predicted in Fig. 3D. Thus, explicit-solvent simulations corroborate the SBS by predicting rapid movement along θ_{S3} after arm dissociation, and support the existence of an SBI.

Discussion and Conclusion

Our simulations report on the initial kinetic events during the HA_2 conformational rearrangement that are observed using explicit-solvent simulations of the complete HA_2 titrated as though in a reduced pH environment. A kinetic ordering suggested by our simulations is 1) HA_1 dissociation, 2) FP removal, 3) arm dissociation, and 4) Loop3-4 disordering and symmetry breaking. This particular ordering is dependent on the specific assumptions we have made, in particular that HA_1 dissociation happens first, and that until HA_1 dissociation, HA_2 maintains a roughly pre-fusion crystallographic configuration. Additionally, we assume that apart from the N-terminal 9 residues (in each monomer) of HA_1 that were explicitly included, the specific interaction between the dissociated HA_1 and HA_2 does not change any of these kinetic events.[9,41] Nevertheless, the existence of HA_1 could delay some events. For example, the C-terminal loop of HA_1 interacts with the FP burial pocket in the crystal structure and in principle could delay the FP dissociation. Also, for some HAs, at least one lobe of HA_1 is attached to a sialic acid receptor, which could change the dynamics for these HAs. Our simulations best represent the majority of HAs that are not attached to receptors. Although allowing for HA_1 interactions may delay or reorder steps 1-3, our simulations still suggest that the fusion competent HA_2 configuration will be prone to symmetry breaking because the FPs and arms must dissociate in order to project the FPs away from HA, and without the stability afforded by the arms and FPs, Loop3-4 is unstable.

The most obvious consequence of Loop3-4 disorder in our simulations was to allow for significant motion of the central coiled-coil S3 (Fig. 3). It seems counterintuitive that HA_2 would bend away from $\theta_{S3} \sim 0$ if its only function is to insert FPs into the host membrane, because this reduces its reach towards the host membrane. We can speculate on the functional consequences of motion in θ_{S3}. First, analogous to the ordering of Loop3-4 after FP dissociation, Loop3-4 disordering may discourage the reassociation of the S1/S4 interface. Second, it provides a hinge for the tilting required to form a meta-stable SBI. Third, motion along θ_{S3} increases the effective range of HA_2 to interact with its neighbors. We expand on the second and third possibilities below.

The post-fusion structure with its S3–S5 interface, models of hemifusion,[3] and recent results from simplified protein models all agree that HA_2 must bend back on itself during the fusion process. Loop3-4 disordering suggests that this symmetry-breaking event may occur very early in the HA_2 rearrangement, even before insertion of the FPs into a membrane. In a scenario where motion along θ_{S3} allows the formation of a meta-stable SBI (Fig. 3B), S3 is effectively locked in an orientation close to parallel to the viral membrane. Such a configuration would bring FPs closer to viral membrane, before they have been inserted into the host membrane. This leads to a possible “cooperative” route[10] for HA_2 to guide membrane fusion (Fig. 4). Along this route, the FPs are shared between the viral and host membranes, and the full free energy of forming the S1–S3 helical bundle can be used to drive the membranes together. A more traditional “sequential” route, closely related to the “spring-loaded” model,[42,43] has all three FPs inserted into the host membrane. In addition, recent experiments showed that S2, the loop region connecting S1 and S3 had affinity to membranes.[44] This leaves open the possibility for S2 to engage into membranes after FPs insertion, to further disrupt lipid structure and facilitate membrane fusion, similar to a scheme proposed for the HIV-1 envelope glycoprotein.[45,46] This scenario involves the melting of any S2 quaternary structure, as in the presented cooperative route.

Beyond providing the possibility for FP insertion into the viral membrane, motion along θ_{S3} increases the effective range of HA_2 to interact with its neighbors. Kinetic models derived from experimental assays of viral membrane fusion kinetics predict that at least 3 HA_2 must cooperate for a successful fusion.[3,47] Additionally, in vitro studies have shown that HA_2 can aggregate.[48] The motion along θ_{S3} would extend the potential radius of interaction between HA_2 molecules. For example, in the case where S1 and S2 are α-helical, $\theta_{S3} = 90°$ would extend the fusion peptides 17 nm further in the plane of the viral membrane, and $\theta_{S3} = 60°/120°$ would extend 14 nm further, compared to $\theta_{S3} = 0°$ as in the pre-fusion crystal structure.

In summary, we observe that at pH 4.5–5.0, FP release strongly depends on protonation of ASP_{112}, which breaks a salt bridge formed with the N-terminus and allows the release of a FP on the microsecond timescale. Apart from the FPs, the HA_2 pre-fusion structure is stable on the microsecond timescale. After the dissociation of S1/S2 from the HA_2 stalk, the subsequent disordering of Loop3-4 is consistent with secondary structure predictors and corroborates the findings of simplified models. Thus, we provide further evidence for a order-disorder transition of Loop3-4 and show that it leads to large motions of the HA_2 regions distal to the viral membrane. This motion is consistent with the formation of a

symmetry-broken intermediate early in the fusion process. Due to the extension of such an intermediate in the plane of the virus, there is an interesting possibility that it can play a role in providing HA_2 spatial aggregation. Experimentally identifying an SBI is well within the capabilities of FRET, TIRF, pH-jump and FTIR,[49] though in vitro preparation of pre-fusion HA_2 remains challenging. Such experiments could monitor either the S3–S5 distance or the S3 distance from the viral surface, both of which undergo large changes upon symmetry-breaking.

Supplementary Material

Refer to Web version on PubMed Central for supplementary material.

Acknowledgments

This work is supported by the Center for Theoretical Biological Physics sponsored by the NSF (Grant PHY-1427654) and by NSF-CHE 1614101. JNO is a CPRIT Scholar in Cancer Research sponsored by the Cancer Prevention and Research Institute of Texas. JKN is a Humboldt Postdoctoral Fellow and was supported in part by the Welch Foundation (Grant C-1792). XL is supported by the National Institute of Health Grant R01-GM110310. JM is supported by National Institutes of Health Grant R01-GM067801, R01-GM116280, National Science Foundation Grant MCB-0818353, and the Welch Foundation (Q-1512). QW is supported by the National Institute of Health Grant R01-AI067839, R01-GM116280, and the Welch Foundation (Q-1826). Anton computer time (Grant PSCA14037P) was provided by the Pittsburgh Supercomputing Center (PSC) through Grant R01-GM116961 from the National Institutes of Health. The Anton machine at PSC was generously made available by D.E. Shaw Research. This work used the Extreme Science and Engineering Discovery Environment (XSEDE), which is supported by National Science Foundation grant number ACI-1053575.

References

1. Skehel JJ, Wiley DC. Receptor Binding and Membrane Fusion in Virus Entry: The Influenza Hemagglutinin. Annual Review of bioc. 2000; 69:531–569.
2. White JM, Delos SE, Brecher M, Schornberg K. Structures and Mechanisms of Viral Membrane Fusion Proteins: Multiple Variations on a Common Theme. Critical Reviews in bioc and Molecular Biology. 2008; 43:189–219.
3. Harrison SC. Viral Membrane Fusion. Virology. 2015; 479:498–507. [PubMed: 25866377]
4. Ekiert DC, Bhabha G, Elsliger MA, Friesen RHE, Jongeneelen M, Throsby M, Goudsmit J, Wilson IA. Antibody Recognition of a Highly Conserved Influenza Virus Epitope. Science. 2009; 324:246–251. [PubMed: 19251591]
5. Ekiert DC, Friesen RHE, Bhabha G, Kwaks T, Jongeneelen M, Yu W, Ophorst C, Cox F, Korse HJWM, Brandenburg B, et al. A Highly Conserved Neutralizing Epitope on Group 2 Influenza A Viruses. Science. 2011; 333:843–850. [PubMed: 21737702]
6. Impagliazzo A, Milder F, Kuipers H, Wagner MV, Zhu X, Hoffman RMB, van Meersbergen R, Huizingh J, Wanningen P, Verspuij J, et al. A Stable Trimeric Influenza Hemagglutinin Stem as a Broadly Protective Immunogen. Science. 2015; 349:1301–1306. [PubMed: 26303961]
7. Wilson IA, Skehel JJ, Wiley DC. Structure of the Hemagglutinin Membrane Glycoprotein of Influenza-Virus at 3-A Resolution. Nature. 1981; 289:366–373. [PubMed: 7464906]
8. Bullough PA, Hughson FM, Skehel JJ, Wiley DC. Structure of Influenza Hemagglutinin at the PH of Membrane-Fusion. Nature. 1994; 371:37–43. [PubMed: 8072525]
9. Chen J, Skehel JJ, Wiley DC. N- and C-Terminal Residues Combine in the Fusion-Ph Influenza Hemagglutinin Ha(2) Subunit to Form an N Cap that Terminates the Triple-Stranded Coiled Coil. Proc Natl Acad Sci U S A. 1999; 96:8967–8972. [PubMed: 10430879]
10. Lin X, Eddy NR, Noel JK, Whitford PC, Wang Q, Ma J, Onuchic JN. Order and Disorder Control the Functional Rearrangement of Influenza Hemagglutinin. Proc Natl Acad Sci U S A. 2014; 111:12049–12054. [PubMed: 25082896]

11. Lorieau JL, Louis JM, Bax A. The Complete Influenza Hemagglutinin Fusion Domain Adopts a Tight Helical Hairpin Arrangement at the Lipid:Water Interface. Proc Natl Acad Sci U S A. 2010; 107:11341–11346. [PubMed: 20534508]
12. Wang QH, Cheng F, Lu MY, Tian X, Ma JP. Crystal Structure of Unliganded Influenza B Virus Hemagglutinin. Journal of Virology. 2008; 82:3011–3020. [PubMed: 18184701]
13. Huang Q, Opitz R, Knapp EW, Herrmann A. Protonation and Stability of the Globular Domain of Influenza Virus Hemagglutinin. Biophys J. 2002; 82:1050–1058. [PubMed: 11806944]
14. Zhou Y, Wu C, Zhao L, Huang N. Exploring the Early Stages of The pH-Induced Conformational Change of Influenza Hemagglutinin. Proteins-Structure Function and bioi. 2014; 82:2412–2428.
15. Noel JK, Schug A, Verma A, Wenzel W, Garcia AE, Onuchic JN. Mirror Images as Naturally Competing Conformations in Protein Folding. Journal of Physical Chemistry B. 2012; 116:6880–6888.
16. Singh JP, Whitford PC, Hayre NR, Onuchic J, Cox DL. Massive Conformation Change in the Prion Protein: Using Dual-Basin Structure-Based Models to Find Misfolding Pathways. Proteins-Structure Function and bioi. 2012; 80:1299–1307.
17. Lee MS, Salsbury FR, Brooks CL. Constant-PH Molecular Dynamics Using Continuous Titration Coordinates. Proteins-Structure Function and bioi. 2004; 56:738–752.
18. Li H, Robertson AD, Jensen JH. Very Fast Empirical Prediction and Rationalization of Protein pKa Values. Proteins-Structure Function and bioi. 2005; 61:704–721.
19. Chem ZP. Versuch Einer Mathematischen Theorie Der Koagulationskinetik Kolloider Lösungen. Z Phys Chem. 1917; 92:129–168.
20. Dorsaz N, De Michele C, Piazza F, De Los Rios P, Foffi G. Diffusion-Limited Reactions in Crowded Environments. Phys Rev Lett. 2010; 105
21. Shaw DE, et al. Millisecond-Scale Molecular Dynamics Simulations on Anton. Proceedings of the ACM/IEEE Conference on Supercomputing (SC09). 2009
22. Piana S, Lindorff-Larsen K, Shaw DE. How Robust are Protein Folding Simulations with Respect to Force Field Parameterization? Biophys J. 2011; 100:L47–L49. [PubMed: 21539772]
23. Lippert RA, Predescu C, Ierardi DJ, Mackenzie KM, Eastwood MP, Dror RO, Shaw DE. Accurate and Efficient Integration for Molecular Dynamics Simulations at Constant Temperature and Pressure. Journal of Chemical Physics. 2013; 139
24. Nose S. A Unified Formulation of the Constant Temperature Molecular-Dynamics Methods. Journal of Chemical Physics. 1984; 81:511–519.
25. Hoover WG. Canonical Dynamics - Equilibrium Phase-Space Distributions. Physical Review A. 1985; 31:1695–1697.
26. Martyna GJ, Tuckerman ME, Tobias DJ, Klein ML. Explicit Reversible Integrators for Extended Systems Dynamics. Molecular Physics. 1996; 87:1117–1157.
27. Shan YB, Klepeis JL, Eastwood MP, Dror RO, Shaw DE. Gaussian Split Ewald: A Fast Ewald Mesh Method for Molecular Simulation. Journal of Chemical Physics. 2005; 122
28. Day R, Bennion BJ, Ham S, Daggett V. Increasing Temperature Accelerates Protein Unfolding without Changing the Pathway of Unfolding. J Mol Biol. 2002; 322:189–203. [PubMed: 12215424]
29. Abraham MJ, Murtola T, Schulz R, Páll S, Smith JC, Hess B, Lindahl E. GROMACS: High Performance Molecular Simulations through Multi-level Parallelism from Laptops to Supercomputers. SoftwareX. 2015; 1–2:19–25.
30. Darden T, York D, Pedersen L. Particle Mesh Ewald - an N. Log(N) Method for Ewald Sums in Large Systems. Journal of Chemical Physics. 1993; 98:10089–10092.
31. Bussi G, Donadio D, Parrinello M. Canonical Sampling through Velocity Rescaling. Journal of Chemical Physics. 2007; 126
32. Parrinello M, Rahman A. Polymorphic Transitions in Single-Crystals - A New Molecular-Dynamics Method. Journal of Applied Physics. 1981; 52:7182–7190.
33. Nose S, Klein ML. Constant Pressure Molecular-Dynamics for Molecular-Systems. Molecular Physics. 1983; 50:1055–1076.

34. Humphrey W, Dalke A, Schulten K. VMD: Visual Molecular Dynamics. Journal of Molecular Graphics and Modelling. 1996; 14:33–38.
35. Daniels RS, Downie JC, Hay AJ, Knossow M, Skehel JJ, Wang ML, Wiley DC. Fusion Mutants of the Influenza-Virus Hemagglutinin Glycoprotein. cell. 1985; 40:431–439. [PubMed: 3967299]
36. Steinhauer DA, Martin J, Lin YP, Wharton SA, Oldstone MBA, Skehel JJ, Wiley DC. Studies Using Double Mutants of the Conformational Transitions in Influenza Hemagglutinin Required for its Membrane Fusion Activity. Proc Natl Acad Sci U S A. 1996; 93:12873–12878. [PubMed: 8917512]
37. Ivanovic T, Choi JL, Whelan SP, van Oijen AM, Harrison SC. Influenza-Virus Membrane Fusion by Cooperative Fold-Back of Stochastically Induced Hemagglutinin Intermediates. Elife. 2013; 2:e00333. [PubMed: 23550179]
38. Ivanovic T, Harrison SC. Distinct Functional Determinants of Influenza Hemagglutinin-Mediated Membrane Fusion. ELife. 2015; 4:e11009. [PubMed: 26613408]
39. Frishman D, Argos P. Knowledge-Based Protein Secondary Structure Assignment. Proteins-Structure Function and Genetics. 1995; 23:566–579.
40. Jones DT. Protein Secondary Structure Prediction Based on Position-Specific Scoring Matrices. J Mol Biol. 1999; 292:195–202. [PubMed: 10493868]
41. Chen J, Wharton SA, Weissenhorn W, Calder LJ, Hughson FM, Skehel JJ, Wiley DC. A Soluble Domain of the Membrane-Anchoring Chain of Influenza Virus Hemagglutinin (Ha(2)) Folds in Escherichia Coli into the Low-Ph-Induced Conformation. pnas of the United States of America. 1995; 92:12205–12209.
42. Carr CM, Kim PS. A Spring-Loaded Mechanism for the Conformational Change of Influenza Hemagglutinin. cell. 1993; 73:823–832. [PubMed: 8500173]
43. Carr CM, Chaudhry C, Kim PS. Influenza Hemagglutinin is Spring-Loaded by a Metastable Native Conformation. Proc Natl Acad Sci U S A. 1997; 94:14306–14313. [PubMed: 9405608]
44. Yu YG, King DS, Shin YK. Insertion of a Coiled-Coil Peptide from Influenza-Virus Hemagglutinin into Membranes. Science. 1994; 266:274–276. [PubMed: 7939662]
45. Roche J, Louis JM, Grishaev A, Ying JF, Bax A. Dissociation of the Trimeric Gp41 Ectodomain at the Lipid-Water Interface Suggests an Active Role in Hiv-1 Env-Mediated Membrane Fusion. pnas of the United States of America. 2014; 111:3425–3430.
46. Dai Z, Tao YS, Liu NN, Brenowitz MD, Girvin ME, Lai JR. Conditional Trimerization and Lytic Activity of Hiv-1 Gp41 Variants Containing the Membrane-Associated Segments. Biochemistry. 2015; 54:1589–1599. [PubMed: 25658332]
47. Danieli T, Pelletier SL, Henis YI, White JM. Membrane Fusion Mediated by the Influenza Virus Hemagglutinin Requires the Concerted Action of at Least Three Hemagglutinin Trimers. Journal of cell Biology. 1996; 133:559–569. [PubMed: 8636231]
48. Epand RF, Yip CM, Chernomordik LV, LeDuc DL, Shin YK, Epand RM. Self-Assembly of Influenza Hemagglutinin: Studies of Ectodomain Aggregation by in Situ Atomic Force Microscopy. Biochimica Et Biophysica Acta-Biomembranes. 2001; 1513:167–175.
49. Causgrove TP, Dyer RB. Nonequilibrium Protein Folding Dynamics: Laser-Induced pH-Jump Studies of the Helix-Coil Transition. Chemical Physics. 2006; 323:2–10.

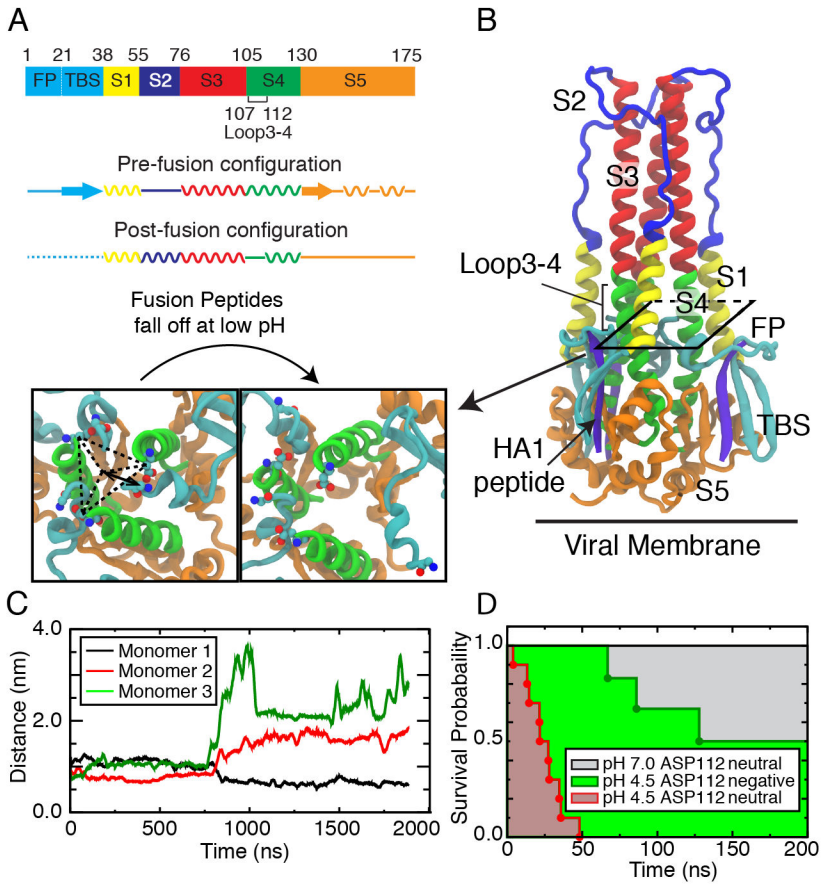

Figure 1.

An electrostatic environment induced by lowered pH increases the rate of FP release. **(A)** Schematic diagram showing the change of secondary structure of a monomer between the pre- and post-fusion crystal structures. The corresponding crystal structures are shown in the supplemental information. The sequence is partitioned into sections differentiated by their structural change in the HA_2 rearrangement, with FP beginning at the N-terminus and S5 ending at the C-terminus. Not shown is an additional C-terminal trans-membrane domain. FP (residue ID 1–20) and TBS (two beta-strands, residue ID 21 to 37) are hydrophobic domains at the N-terminus. They are missing in the post-fusion crystal structure.[8] S1 (residue ID 38 to 54, yellow) and S3 (residue ID 76 to 104, red) maintain their secondary structure. S2 (residue ID 55 to 75, blue) changes from a loop to helix. S4 (residue ID 105 to 129, green) and S5 (residue ID 130 to 175, orange) have a partial secondary structure shift. Loop3-4 (residue ID 107 to 112) is a region of low helical propensity at S3–S4 interface that undergoes a helix-loop transition. **(B)** Pre-fusion HA_2 crystal structure (PDB ID: 2HMG) shows the FPs to be buried in a hydrophobic pocket within S4. 3 N-terminal peptides of HA_1 (one for each monomer, residue ID 10 to 18 of HA_1, violet) are disulfide bonded to S5. The inset magnifies a view of the FPs in the crystal and after dissociation during the simulation, with N-termini of FPs and ASP_{112} shown as spheres.[34] The left inset defines the geometric center of the hydrophobic pocket as the center of mass of the three ASP_{112} in the crystal. **(C)** The distance between the N-terminus of each FP and the center of the hydrophobic pocket.

The curves are averaged over a 0.5 ns window for clarity. **(D)** The survival probability for the release of the first FP at high temperature (T = 398K) plotted as a function of time for the cases with neutral (red filled, 10 runs) and negative (green filled, 7 runs) ASP_{112}. Also shown are control simulations (grey filled, 6 runs) with neutral ASP_{112} at pH 7.

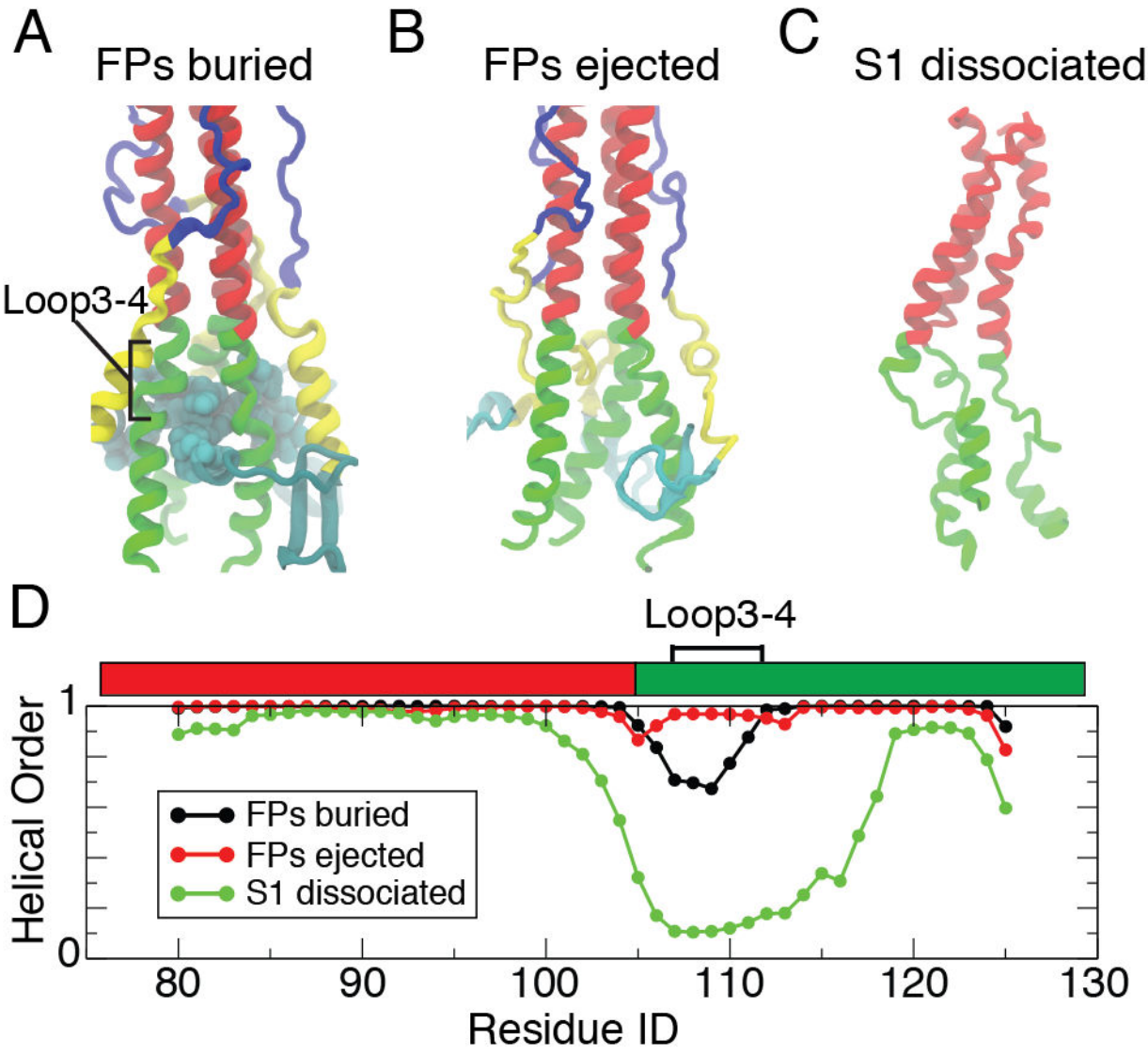

Figure 2.

Helical order of domains S3/S4 during different stages of the conformational rearrangement. Representative snapshots highlighting the structure of regions contacting Loop3-4 are shown for HA_2 **(A)** before FP release, **(B)** after FP release, and **(C)** after the dissociation of S1/S2. **(D)** The helical order of a residue is determined by averaging over the three monomers the probability that the STRIDE algorithm[39] determines an alpha helical secondary structure. The black curve is averaged over a 700 ns simulation at pH 4.5 started from the crystal structure, before dissociation of the FP and corresponding to (A). The red curve is averaged for a 2 μs at pH 5 where the FPs are already ejected, corresponding to (B). The green curve is 6 μs of simulation after the deletion of S1/S2. Loop3-4 shows substantial disorder compared with the other parts of S3/S4.

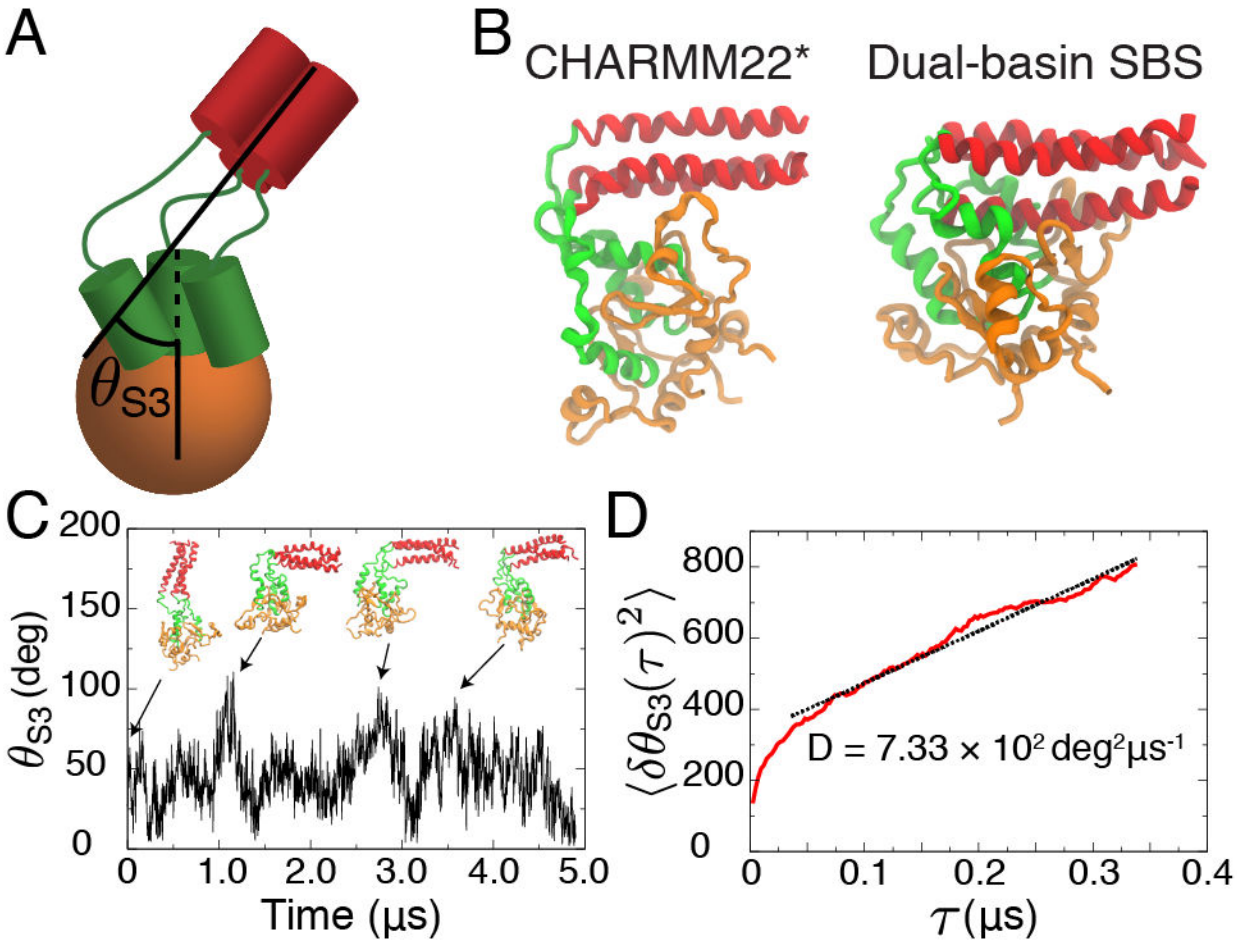

Figure 3.

Disordering of Loop3-4 upon breaking of the S1–S4 interface leads to large fluctuations in HA_2. **(A)** The coordinate θ_{S3} estimates the deviation of S3 from a perpendicular orientation to the viral surface by measuring the angle the coiled-coil makes relative to S5. S5 is anchored to the viral membrane by a C-terminal transmembrane region. **(B)** Two possible structures for an SBI taken from explicit-solvent simulations and dual-basin SBS (see 2 Basins C, E and F in ref.[10] for explanation of the SBS results). **(C)** θ_{S3} as a function of time during the final 5 μs of a constant temperature (310K) simulation of HA_2 with S1 and S2 removed. **(D)** Effective diffusion coefficient is obtained from the mean square displacement of the angle $\langle \delta\theta_{S3}(\tau)^2 \rangle$ in the diffusive regime. Linear fitting is drawn as a black dashed line.

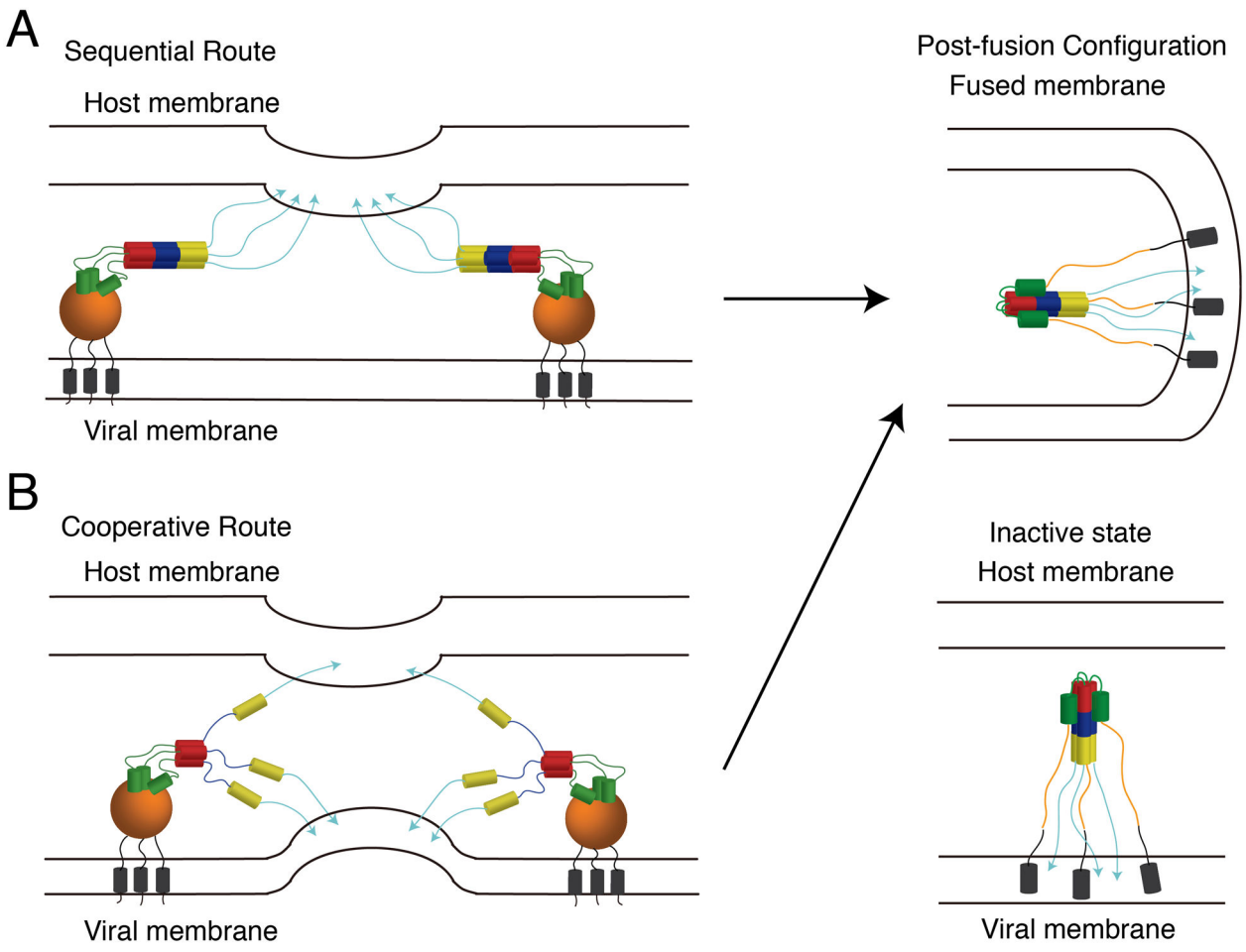

Figure 4.

A cartoon illustration of possible fusogenic routes for HA_2 from a symmetry-broken intermediate (SBI). **(A)** A "sequential route" where three FPs of each HA_2 are inserted into host membranes. This route is called sequential because the arms fold into their post-fusion coiled-coil before the membranes are brought together. This resembles the "spring-loaded" model.[42,43] **(B)** A "cooperative route" where the FPs are inserted into both the host and viral membranes. The SBI facilitates this route by bringing the FPs closer to viral membrane. This route is termed cooperative because the coiled-coil forms only as the membranes are brought close together. In both of these routes, S5 will eventually melt and wrap around HA_2, presumably helping to bring two membranes together. If S5 breaks before at least one FP is inserted into the host membrane, likely all the FPs are pinned at the viral surface leading to a inactive conformational transition.[10,38]